Modified embedded-atom method interatomic potential for the Fe–Al system

2010 J. Phys.: Condens. Matter 22 175702

(http://iopscience.iop.org/0953-8984/22/17/175702)

IOP Publishing Journal of Physics: Condensed Matter

J. Phys.: Condens. Matter **22** (2010) 175702 (9pp) doi:10.1088/0953-8984/22/17/175702

Modified embedded-atom method interatomic potential for the Fe–Al system

Eunkoo Lee and Byeong-Joo Lee[1]

Department of Materials Science and Engineering, Pohang University of Science and Technology (POSTECH), Pohang 790-784, Republic of Korea

E-mail: calphad@postech.ac.kr (B-J Lee)

Received 7 January 2010, in final form 25 February 2010
Published 12 April 2010
Online at stacks.iop.org/JPhysCM/22/175702

Abstract

An interatomic potential for the Fe–Al binary system has been developed based on the modified embedded-atom method (MEAM) potential formalism. The potential can describe various fundamental physical properties of Fe–Al binary alloys—structural, elastic and thermodynamic properties, defect formation behavior and interactions between defects—in reasonable agreement with experimental data or higher-level calculations. The applicability of the potential to atomistic investigations of various defect formation behaviors and their effects on the mechanical properties of high aluminum steels as well as Fe–Al binary alloys is demonstrated.

(Some figures in this article are in colour only in the electronic version)

1. Introduction

Manganese–aluminum-carbon steels with high aluminum contents, which have been regarded as a substitute for chromium–nickel stainless steels, are now attracting renewed academic and industrial interest due to their light weight [1]. Since mechanical twinning was found to be the main deformation mechanism for this class of steels [2], detailed investigations on the twinning induced plasticity (TWIP) phenomenon have been carried out [3]. Even though the stacking fault energy (SFE) is being mentioned as a key factor in the twinning, because of the difficulty of and uncertainty in the experimental measurements of the SFE, information about the SFE in TWIP steels and the effect of alloying elements on it is very limited.

Aluminum is also characterized as an element that causes a DO_3 or B2 ordering in a wide composition range when alloyed to iron. It is well known that ordered compounds are brittle [4, 5]. It is also known that various point defects such as vacancies and anti-site atoms exist in different proportions depending on the deviation from stoichiometry in the B2 ordered Fe–Al alloys [6]. Even though it has been observed that those point defects have a strong effect on the plasticity of the Fe–Al ordered alloys, more details about the distribution and role of individual point defects and their clusters in the plastic deformation behavior of alloys of various composition are not known.

In order to further improve the mechanical properties of high Al steels as a structural material, it would be necessary to understand the formation behavior of various point defects and their effects on twin formation at a more fundamental level. All those are atomic scale phenomena which are difficult to examine experimentally but which can be best investigated using atomistic simulation techniques. First-principles calculations provide the most reliable information on materials properties at atomic or sub-atomic scales. However, due to the size (or number of atoms) limit, it is often not possible to investigate material behaviors using only first-principles calculations. Another approach is to use (semi-)empirical interatomic potentials, which can deal with more than a million atoms. Here, it is important that the interatomic potential should be able to reproduce correctly various fundamental physical properties (thermodynamic, elastic, defect and ordering properties, etc, in the case of the Fe–Al alloy system) of relevant materials systems.

Because of the importance of atomistic simulation approaches to the mechanical properties of Fe–Al alloys, many interatomic potential models have indeed been developed not only based on pair-potential formalisms [7–10] but also on many-body potential formalisms such as the embedded-atom method (EAM) [11, 12] and the modified analytic EAM [13]. All the many-body interatomic potentials reproduce fundamental physical properties of the Fe–Al alloys

[1] Author to whom any correspondence should be addressed.

reasonably well. However, none of the potentials have been applied to Fe–C and Fe–Mn systems which should be included when considering practical Fe–Mn–Al–C systems.

To the best knowledge of the present authors, the second nearest-neighbor modified EAM (2NN MEAM) [14, 15] is a unique potential formalism which has been applied to the relevant elements, iron [15], manganese [17], aluminum [16] and carbon [18], and their alloy systems, Fe–C [19] and Fe–Mn [17]. As a starting point to investigate the effect of aluminum on the defect formation and plastic deformation behavior in high Al steels (Fe–Mn–Al–C) at an atomic scale, the purpose of the present work is to develop a 2NN MEAM interatomic potential for the Fe–Al alloy system. Special attention was paid to reproducing the structural, thermodynamic, elastic, defect and ordering properties of the alloys.

In the present paper, the 2NN MEAM formalism for alloy systems and the procedure for determining the potential parameters are briefly outlined. Then, how well the potential can describe the fundamental physical properties of relevant materials is demonstrated by comparing the MEAM calculations with experimental data or other calculations. The applicability of the present potential for atomistic simulations to investigate the defect formation and deformation behavior of Fe–Al alloys is also discussed.

2. Formalism

2.1. Potential formalism

In the MEAM, the total energy of a system is approximated as

$$E = \sum_i \left[F_i(\bar{\rho}_i) + \tfrac{1}{2} \sum_{j(\neq i)} S_{ij}\phi_{ij}(R_{ij}) \right]. \tag{1}$$

F_i is the embedding function for an atom i embedded in a background electron density $\bar{\rho}_i$, and S_{ij} and $\phi_{ij}(R_{ij})$ are, respectively, the screening function and the pair interaction between atoms i and j separated by a distance R_{ij}. For energy calculations, the functional forms for F_i and ϕ_{ij} should be given. The background electron density at each atomic site is computed considering the directionality of bonding, i.e. by combining several partial electron density terms for different angular contributions. A specific form is given to the embedding function F_i but not to the pair interaction ϕ_{ij}. Instead, a reference structure where individual atoms are on exact lattice points is defined and the total energy per atom of the reference structure is estimated from the zero-temperature universal equation of state by Rose *et al* [20]. Then, the value of the pair interaction is evaluated from the known values of the total energy per atom and the embedding energy as a function of the nearest-neighbor distance. In the original MEAM [21], only first nearest-neighbor interactions are considered. The second and more distant nearest-neighbor interactions are neglected by the use of a strong, many-body screening function [22]. Consideration of the second nearest-neighbor interactions in the modified formalism (2NN MEAM [14, 15]) is effected by adjusting the screening parameters $C_{\min}$ so that the many-body screening becomes less severe. In addition, a radial cutoff function [22] is applied to reduce calculation time. Details of the MEAM formalism have been published in the literature [14, 15, 21, 22] and will not be repeated here.

To describe an alloy system, the pair interaction between different elements should be determined. For this, a similar technique that is used to determine pair interaction for elements is applied to binary alloy systems. A perfectly ordered binary intermetallic compound, where one type of atom has only the same types of atoms as second nearest-neighbors, is considered as a reference structure. For the Fe–Al system, a Fe_3Al-type $L1_2$ ordered structure was chosen as the reference structure. For the $L1_2$ Fe_3Al structure, the total energy per atom (for 3/4Fe atom + 1/4Al atom) is given as follows:

$$\begin{aligned} E^{\mathrm{u}}_{\mathrm{Fe_3Al}}(R) &= \tfrac{3}{4}F_{\mathrm{Fe}}(\bar{\rho}_{\mathrm{Fe}}) + \tfrac{1}{4}F_{\mathrm{Al}}(\bar{\rho}_{\mathrm{Al}}) \\ &\quad + \frac{Z_1}{2}\left[\frac{1}{2}\phi_{\mathrm{FeAl}}(R) + \frac{1}{2}\phi_{\mathrm{FeFe}}(R)\right] \\ &\quad + \frac{Z_2}{2}\left[\frac{3}{4}S_{\mathrm{Fe}}\phi_{\mathrm{FeFe}}(aR) + \frac{1}{4}S_{\mathrm{Al}}\phi_{\mathrm{AlAl}}(aR)\right], \end{aligned} \tag{2}$$

where Z_1 and Z_2 are the numbers of first and second nearest-neighbors in the $L1_2$ Fe_3Al structure, respectively. In the present case, Z_1 and Z_2 are 12 and 6, respectively. S_{Fe} and S_{Al} are the screening function for the second nearest-neighbor interactions between Fe atoms and between Al atoms, respectively, and a is the ratio between the second and first nearest-neighbor distances in the reference structure. The pair interaction between Fe and Al can now be obtained in the following form:

$$\begin{aligned} \phi_{\mathrm{FeAl}}(R) &= \tfrac{1}{3}E^{\mathrm{u}}_{\mathrm{Fe_3Al}}(R) - \tfrac{1}{4}F_{\mathrm{Fe}}(\bar{\rho}_{\mathrm{Fe}}) - \tfrac{1}{12}F_{\mathrm{Al}}(\bar{\rho}_{\mathrm{Al}}) \\ &\quad - \phi_{\mathrm{FeFe}}(R) - \tfrac{3}{4}S_{\mathrm{Fe}}\phi_{\mathrm{FeFe}}(aR) - \tfrac{1}{4}S_{\mathrm{Al}}\phi_{\mathrm{AlAl}}(aR). \end{aligned} \tag{3}$$

The embedding functions F_{Fe} and F_{Al} can be readily computed [14, 15, 21, 22]. The pair interactions ϕ_{FeFe} and ϕ_{AlAl} between the same types of atoms can also be computed from descriptions of individual elements. To obtain $E^{\mathrm{u}}_{\mathrm{Fe_3Al}}(R)$, the universal equation of state [20] should be considered once again for the $L1_2$ Fe_3Al as follows:

$$E^{\mathrm{u}}(R) = -E_{\mathrm{c}}(1 + a^* + da^{*3})\mathrm{e}^{-a^*}, \tag{4}$$

where d is an adjustable parameter

$$a^* = \alpha(R/r_{\mathrm{e}} - 1), \tag{5}$$

and

$$\alpha = \left(\frac{9B\Omega}{E_{\mathrm{c}}}\right)^{1/2}. \tag{6}$$

r_{e} is the equilibrium nearest-neighbor distance, E_{c} is the cohesive energy, B is the bulk modulus and Ω is the equilibrium atomic volume of the reference structure. The parameters E_{c}, r_{e} (or Ω), B and d in the universal equation of state are assumed or determined from relevant experimental data or high-level calculations. The pair interaction between Fe and Al is then determined as a function of the interatomic distance R.

Table 1. 2NN MEAM parameters for pure Fe and Al. The units of the cohesive energy E_c, equilibrium nearest-neighbor distance r_e and bulk modulus B are eV, Å and 10^{12} dyne cm^{-2}, respectively.

	E_c	R_e	B	A	$\beta^{(0)}$	$\beta^{(1)}$	$\beta^{(2)}$	$\beta^{(3)}$	$t^{(1)}$	$t^{(2)}$	$t^{(3)}$	C_{max}	C_{min}	d
Fe	4.29	2.48	1.730	0.56	4.15	1.0	1.0	1.0	2.6	1.8	−7.2	2.80	0.36	0.05
Al	3.36	2.86	0.794	1.16	3.20	2.6	6.0	2.6	3.05	0.51	7.75	2.80	0.49	0.05

2.2. Determination of potential parameters

The MEAM for an alloy system is based on the MEAM potentials of the constituent elements. In the present work, the MEAM parameters for Fe and Al were taken from Lee *et al* [15, 16] without any modification. The potential parameters for pure Fe and Al are listed in table 1.

As described in the previous section, the extension of the MEAM to an alloy system involves the determination of the pair interaction between different types of atoms. The main task is to estimate the potential parameters of the universal equation of state for the reference structure. Equations (4)–(6) show that the potential parameters are E_c, r_e (or Ω), B and d. The first three are material properties if the reference structure is a real phase structure that exists on the phase diagram of the relevant system. Experimental data for that phase can be used directly. Otherwise, the parameter values should be optimized so that experimental information on other phases or first-principles calculation results which are widely used to obtain fundamental physical and thermodynamic properties can be reproduced, if available, or assumptions should be made. The fourth parameter, d, is a model parameter. The value can be determined by fitting to the $(\partial B/\partial P)$ value of the reference structure. When the reference structure is not a real phase, it is difficult to estimate a reasonable value. For such alloy systems, d is given the average value of those for the pure constituent elements.

In addition to the parameters for the universal equation of state, two model parameters, C_{min} and C_{max}, must be determined to describe alloy systems. As can be seen in table 1, each element has its own value of C_{min} and C_{max}. C_{min} and C_{max} determine the extent of screening of an atom (k) to the interaction between two neighboring atoms (i and j). For pure elements, the three atoms are all of the same type (i–j–k = A–A–A or B–B–B). However, in the case of alloys, one of the interacting atoms and/or the screening atoms can be different types (there are four cases: i–j–k = A–B–A, B–A–B, A–A–B and A–B–B). Different C_{min} and C_{max} values may have to be given in each case. Another model parameter is the atomic electron density scaling factor ρ_0. For an equilibrium reference structure ($R = r_e$), the values of all atomic electron densities become ρ_0. This is an arbitrary value and does not have any effect on calculations for pure elements. This parameter is often omitted when describing the potential model for pure elements. However, for alloy systems, especially for systems where the constituent elements have different coordination numbers, the scaling factor (relative difference) has a great effect on calculations.

The 13 model parameters discussed above, E_c, r_e, B, d, C_{min}, C_{max} and ρ_0 (there are four binary C_{min} and C_{max} parameters), must be determined to describe an alloy system. The optimization of the model parameters is performed by fitting to known physical properties of the alloy system. The parameter values are determined by a systematic trial and error method after the relations between individual parameters and target property values (mostly 0 K values) are found. Several sets of parameters that equally reproduce the target property values are obtained. Those parameter sets are used to calculate thermal properties or properties at finite temperatures such as stability of equilibrium phases, thermal expansion coefficients, order–disorder transition, etc, and the best set is finally selected.

The phase diagram of the Fe–Al binary system is characterized by a large solubility of Al (up to 50 at.% Al) in the body-centered cubic (bcc) solid solution. Over 20 at.% Al, the random bcc solid solution transforms into the B2-FeAl ordered phase at low temperature. The transition temperature increases with increasing Al content. At around 25 at.% Al, the B2 ordered phase further transforms into the DO_3-Fe_3Al ordered phase. The experimental physical properties of the Fe–Al alloys, which are available in the literature and can thus be used to determine potential parameter values, were lattice parameters [23–26], bulk modulus and elastic constants [27] of the above-mentioned ordered and disordered solid solution phases. Enthalpy of formation and enthalpy of mixing were also available for the solid [28–30] and liquid [31, 32] solution phases, respectively. The ordering transition temperature [33] that changes with composition and the vacancy formation energy [34, 35] could be considered to determine the potential parameters or to evaluate the transferability of the potential. First-principles calculations [36–47] and empirical calculations using other many-body potentials [11–13] are also available for various physical properties, and those values were used mainly for comparison. Even though many other compound phases are reported on the Al-rich region of the Fe–Al phase diagram, those phases were not considered in the present work since their crystal structures were unclear or too complicated to deal with using an (semi-)empirical interatomic potential.

The parameter values were determined by fitting to the above-mentioned experimental information on the Fe–Al alloys. It has been mentioned that the first three parameters, E_c, r_e and B, are material properties (the cohesive energy, equilibrium nearest-neighbor distance and bulk modulus of the reference structure, respectively) once the reference structure is a real phase structure that exists on the phase diagram. However, since the reference structure selected in the present study, $L1_2$-Fe_3Al, was not a real phase structure, the above parameter values could not be determined directly from experimental data. The E_c parameter value was optimized so that the enthalpy of formation in solid phases and the enthalpy of mixing in the liquid phase are best reproduced

Table 2. 2NN MEAM parameters for the Fe–Al system optimized in the present work. The units of the formation energy of the reference phase ΔE_c, the equilibrium nearest-neighbor distance r_e and bulk modulus B are eV, Å and 10^{12} dyne cm^{-2}, respectively.

	Selected value	Procedure for the determination
Reference state	$L1_2$-Fe_3Al	
$\Delta E_c(E_c^{L1_2} - 0.75E_c^{Fe} - 0.25E_c^{Al})$	−0.18	Fitting to enthalpy of formation/mixing
r_e	2.59	Fitting to lattice parameters
B	$0.75B^{Fe} + 0.25B^{Al}$	Default assumed value
d	$0.75d^{Fe} + 0.25d^{Al}$	Default assumed value
C_{min} (Fe–Al–Fe)	0.36 ($=C_{min}^{Fe}$)	Default assumed value
C_{min} (Al–Fe–Al)	1.21	Fitting to elastic constants of B2-FeAl
C_{min} (Fe–Fe–Al)	1.00	Fitting to elastic constants of DO_3-Fe_3Al
C_{min} (Fe–Al–Al)	$[0.5\ (C_{min}^{Fe})^{1/2} + 0.5(C_{min}^{Al})^{1/2}]^2$	Default assumed value
ρ_0	$\rho_0^{Fe}/\rho_0^{Al} = 1.0$	Default assumed value

simultaneously. Similarly, the r_e parameter value was optimized so that the composition dependency of the lattice parameter of the bcc solid solutions is best reproduced. The B parameter value could be determined so that the bulk moduli of ordered phases are best reproduced. However, based on previous works on the Fe–Ti and Cu–Zr systems [48, 49], where it was found that the bulk moduli of reference structures approximated by taking a weighted average of the values for pure elements are close to first-principles values, the same approximation (taking the weighted average of the values for pure elements) was made for the B parameter in the present work. As will be shown later, this satisfactorily reproduced the bulk moduli of various ordered phases. The same approximation was also made for the d parameter due to the lack of information.

Among the eight C_{min} and C_{max}, only two C_{min} parameters had effects on the elastic constants of ordered phases and were given non-default values to better describe those properties. In binary systems, the density scaling factors (actually the ratio between those for individual elements) generally affect the composition dependency of enthalpy of formation or mixing. Because a reasonable composition dependency of enthalpy of formation and mixing could be obtained without adjusting the ratio, in the present study the atomic electron density scaling factor ρ_0 values for Fe and Al were assumed to be the same, i.e. the ratio is 1. Table 2 shows the finally determined MEAM parameters for the Fe–Al binary system.

3. Calculation of physical properties

In this section, fundamental physical properties of the Fe–Al alloys will be calculated using the present MEAM potentials shown in tables 1 and 2 and compared with experimental information or other calculations. The 2NN MEAM formalism includes up to second nearest-neighbor interactions. Therefore, the radial cutoff distance during atomistic simulations should be at least larger than the second nearest-neighbor distance in the structures under consideration. All calculations presented here are performed with a radial cutoff distance of 4.0 Å, which is between the second and third nearest-neighbor distances of solid phases. If not designated, all MEAM values shown in this section are those calculated at 0 K.

The properties calculated in the present study can be divided into three groups. One group is the fundamental physical properties: lattice parameters, elastic constants and enthalpy of formation or mixing. Those properties are used for parameter optimization. The comparison between calculation and experimental values shows the quality of fitting. The second group is those properties with experimental information or other calculation values not used for parameter optimization. The B2/A2 order–disorder transition temperature and various point defect formation energies are in this group. Through comparisons between the present calculation and experimental data or other calculations, the transferability of the present potential and its applicability to the investigation of defect formation behavior of ordered Fe–Al alloys can be evaluated. The final group is the properties where only qualitative or no information is available, and includes the effect of Al on the SFE in fcc Fe, the segregation of Al atoms on grain boundaries of bcc Fe and the binding energy between dislocation and an Al solute atom. The calculation of those properties provides information which is helpful for understanding the effect of Al on the mechanical and deformational behavior of Fe–Al alloys. The agreement between the present calculation and quantitative or qualitative experimental information on the second and third groups of properties will also demonstrate the applicability of the present atomistic simulation approach to the investigation of the defect formation and deformation behavior of Fe–Al alloys.

As mentioned above, the first property calculated using the present MEAM potential is the lattice parameters of ordered B2-FeAl, DO_3-Fe_3Al and $L1_2$-Fe_3Al compounds (table 3) and the disordered bcc solid solution (figure 1, where 'x' represents the mole fraction of Al). The calculated bulk modulus and elastic constants of the ordered compounds are compared with experimental data or other calculations in table 4. The enthalpy of formation of ordered compounds and solid solution phases, and the enthalpy of mixing of liquid were also calculated and are compared with relevant experimental data or other calculations in table 5 and figures 2 and 3, respectively.

As shown in tables 3–5 and figures 1–3, the present calculation generally well reproduces the target property values used for parameter optimization. The lattice parameters of the ordered B2, DO_3 and $L1_2$ compounds are reproduced within a 1% error and the deviations from those of B2 and DO_3 compounds have the opposite sign, which indicates that any further improvement would not be obtained by adjusting the r_e value. However, the quality of the calculated elastic constants

Table 3. Calculated lattice parameter of B2, DO_3 and $L1_2$ ordered Fe–Al phases in comparison with experimental data and other calculations. The unit of the lattice parameter is Å.

Phase	MEAM	Expt[a]	First-principles calculations	Empirical potentials
B2-FeAl	2.919	2.90	2.879[b], 2.87[c], 2.900[d], 2.89[e], 2.87[f], 2.83[g], 2.889[h]	2.91[k], 2.90[l], 3.031[m]
DO_3-Fe_3Al	2.879	2.89	2.892[b], 2.88[c], 2.850[d], 2.885[e], 2.895[f], 2.889[h], 2.865[i], 2.889[j]	2.866[l], 2.952[m]
$L1_2$-Fe_3Al	3.669	—	3.669[b], 3.65[c], 3.645[i], 3.657[j]	

[a] Reference [23]. [b] Reference [36]. [c] Reference [37]. [d] Reference [38]. [e] Reference [39]. [f] Reference [40]. [g] Reference [41]. [h] Reference [42]. [i] Reference [43]. [j] Reference [44]. [k] Reference [11]. [l] Reference [12]. [m] Reference [13].

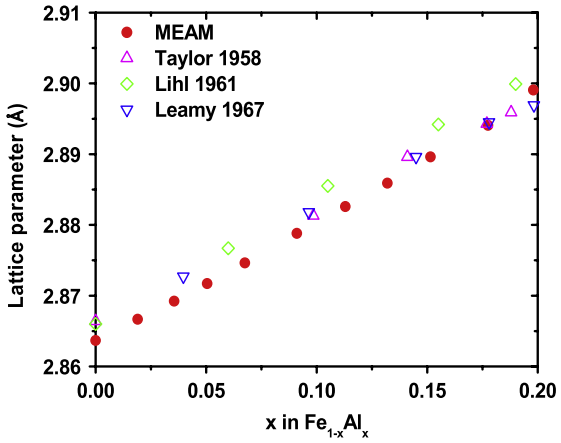

Figure 1. Calculated lattice parameter of disordered bcc Fe–Al alloys, in comparison with experimental data [24–26].

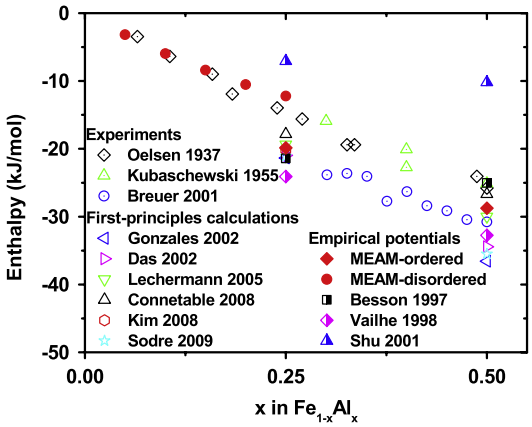

Figure 2. Calculated enthalpy of formation of disordered and DO_3, B2 ordered Fe–Al phases, in comparison with experimental data [28–30], first-principles calculations [36, 37, 39, 40, 42, 43] and calculations using empirical potentials [11–13].

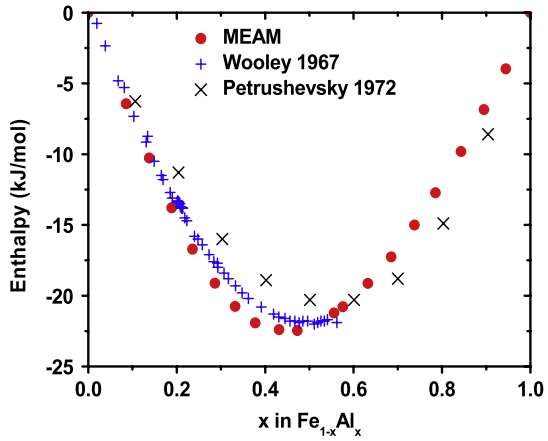

Figure 3. Calculated enthalpy of mixing of the Fe–Al liquid alloys, in comparison with experimental data [31, 32].

is relatively worse, especially the C44 values. It should be mentioned here that actually the calculated C44 values (and all other elastic constants) could be increased toward a better agreement with experimental data by simply increasing the *B* parameter value which was given a default value. However, the present authors wanted to show that a reasonable result (a slightly smaller *B* value for B2 and slightly larger value for DO3 when compared to experimental data) is obtained by using only the default *B* value. If one needs a potential that yields a better agreement with C44 values, one can increase the *B* value by a few per cent.

It is also shown that the thermodynamic properties (enthalpy of formation and enthalpy of mixing) are reproduced well within the scattering range of experimental or first-principles data. Most of the first-principles calculations have predicted the $L1_2$ ordered structure to be more stable than the DO_3 ordered structure contrary to experimental observation, while the present calculation predicts the relative stability of the two structures correctly in agreement with recent first-principles calculations [43, 44].

It has been shown that the MEAM potential parameters are optimized satisfactorily, yielding generally good agreements with target property values. The transferability of the present potential will now be examined by calculating other known properties not used during the parameter optimization procedure, i.e. the order–disorder transition temperature and point defect energy, and comparing with relevant experimental data or other calculations.

As mentioned in the previous section, A2/B2 and A2/B2/DO_3 transitions occur over 20 at.% Al [33]. Transition temperatures can be estimated by monitoring the temperature dependency of the long-range order (LRO) parameter for samples equilibrated using a canonical ensemble Monte Carlo (MC) simulation. For the MC simulation in the present work alloy samples with 2000 atoms ($10 \times 10 \times 10$ unit cells) were prepared for several different alloy compositions. The three-dimensional periodic boundary condition was applied during the MC runs, allowing changes of sample size and thermal vibration of lattice atoms. The elementary step of MC simulation is as follows. Two atoms are randomly chosen and

Table 4. Calculated bulk modulus and elastic constants of B2, DO_3 and $L1_2$ ordered Fe–Al phases in comparison with experimental data and other calculations. In each item, the first line is for B2-FeAl, the second for DO_3 and the third for $L1_2$ Fe_3Al. The unit of bulk modulus and elastic constant is 10^{12} dyne cm^{-2}.

	MEAM	Expt[a]	First-principles calculations	Empirical potentials
Bulk modulus	1.246	1.361	1.72[b], 1.56[c], 1.55[d]	
	1.489	1.441	1.59[b], 1.70[c], 1.51[d], 1.39[e], 1.74[f]	
	1.496	—	1.85[b], 1.68[d], 1.43[e], 1.68[f]	
C11	1.527	1.811	2.70[b], 1.833[c], 2.90[g]	1.413[h], 1.920[i], 2.90[j]
	2.225	1.710	1.64[b], 1.592[c],	1.512[h], 2.62[j]
	1.743	—	1.84[b]	
C12	1.106	1.137	1.05[b], 1.070[c], 1.30[g]	1.354[h], 1.200[i], 1.30[j]
	1.121	1.306	1.27[b], 1.375[c],	1.427[h], 1.56[j]
	1.372	—	1.45[b]	
C44	0.780	1.271	1.52[b], 1.070[c], 1.65[g]	1.106[h], 1.168[i], 1.65[j]
	1.091	1.317	1.42[b], 1.375[c],	1.261[h], 1.62[j]
	0.760	—	1.60[b]	

[a] Reference [27]. [b] Reference [37]. [c] Reference [38]. [d] Reference [36]. [e] Reference [44].
[f] Reference [43]. [g] Reference [41]. [h] Reference [13]. [i] Reference [11]. [j] Reference [12].

Table 5. Calculated enthalpy of formation of ordered Fe–Al phases in comparison with other calculations. The unit of the enthalpy is kJ/gram-atom.

Phase	MEAM	First-principles calculations	Empirical potentials
B2-FeAl	−28.75	−29.98[a], −26.68[b], −36.56[c], −35.52[d], −34.44[e]	−32.75[g], −25.04[h], −10.21[i]
DO_3-Fe_3Al	−19.86	−19.36[a], −17.85[b], −21.35[c], −21.12[d], −20.97[e], −20.13[f]	−24.08[g], −21.43[h], −7.080[i]
$L1_2$-Fe_3Al	−17.34	−21.38[a], −19.19[b], −18.78[f]	

[a] Reference [36]. [b] Reference [37]. [c] Reference [39]. [d] Reference [40]. [e] Reference [42]. [f] Reference [43].
[g] Reference [11]. [h] Reference [12]. [i] Reference [13].

interchanged. Small random displacements in the positions of the two atoms are also attempted. The energy change before and after the trial of transition, ΔE, is calculated and used to evaluate the transition probability P:

$$P = \exp\left(-\frac{\Delta E}{k_B T}\right), \tag{7}$$

where

$$\Delta E = E_{\text{after}} - E_{\text{before}}. \tag{8}$$

This simulation gives an equilibrium atomic configuration for a given Al content, temperature and pressure (zero external pressure). Order–disorder transition temperatures in individual alloys are determined by performing the MC simulation in a temperature range across estimated transition temperatures and identifying the temperature where an abrupt change of LRO parameter occurs. In the present work, a DO_3 LRO parameter was defined as

$$\text{LRO} = \frac{r_{\text{Fe}} - x_{\text{Fe}}}{1 - x_{\text{Fe}}}, \tag{9}$$

where r_{Fe} is the fraction of Fe atoms in the Fe sites of a perfectly ordered DO_3 structure. By this, the LRO of a perfectly ordered DO_3 structure becomes 1 and that of a B2 ordered structure becomes 0.33 for all compositions lower than 50 at.% Al, which means both DO_3 and B2 ordering can be identified using a single LRO parameter. Figure 4 shows LRO versus temperature curves for samples with 25, 35 and 45 at.% Al, obtained by increasing the temperature by 200 K (100 K in the transition temperature region) with 10 000 Monte Carlo steps at each temperature. According to the present potential,

Table 6. Calculated order–disorder transition temperatures with Al content, in comparison with experimental data. The unit of the temperature is K.

	0.25	0.35	0.45
	$DO_3 \rightarrow B2 \rightarrow A2$	$B2 \rightarrow A2$	$B2 \rightarrow A2$
Expt [33]	850–1050	1450	1600
MEAM	1100–1200[a]	1800–1900	1900–2000

[a] For $DO_3 \rightarrow A2$ transition.

the Fe–25 at.% Al alloy is DO_3 ordered at low temperature while the 35 at.% and 45 at.% Al alloys are B2 ordered. Because exact calculation of the transition temperatures was not the purpose of the present study, the transition temperatures at individual alloy compositions were roughly obtained in a form of a range between the two temperatures where the decrease of LRO starts and ends, and are given in table 6. The calculated transition temperature ranges are generally higher than experimental data. This is partly because the disordering transition was observed during heating (10 000 MCS may not be enough to obtained full equilibrium at each temperature) and partly because of overestimation of the present MEAM for the melting point of pure Fe by about 250 K [15]. It should also be mentioned here that actually DO3 → B2 → A2 disordering was expected for the Fe–25 at.% Al alloy. However, probably because of the large temperature interval (100 K) used in the MC simulation, the B2 ordering could not be detected in the present study.

Even though the transition temperatures are generally overestimated, it has been shown that the present interatomic

Table 7. Calculated point defect formation energy in the B2-FeAl phase, in comparison with experimental data or other calculations. The point defects considered are vacancy and anti-site formation in Fe and Al site. The unit of the energy is eV.

	MEAM	Expt[a,b]	Vailhe[c]	Besson[d]	Shu[e]	Kellou[f]	Fu[g]	Fähnle[h]	Bakker[i]
$E_f^{vac,Al}$	1.51		1.28	2.8	1.78	4.70	4.00	3.46	1.49
$E_f^{vac,Fe}$	1.29	∼1.0	1.26	0.8	1.06	1.47	0.97	1.06	0.65
$E_f^{anti,Al}$	0.59		−0.75	0.78	0.27	0.75	0.95	0.99	0.95
$E_f^{anti,Fe}$	0.59		1.87	0.76	0.50	1.09	1.03	0.99	1.03

[a] Reference [34]. [b] Reference [35]. [c] Reference [11], embedded-atom method. [d] Reference [12], embedded-atom method. [e] Reference [13], modified analytic embedded-atom method.
[f] Reference [45], first-principles calculation. [g] Reference [46], first-principles calculation.
[h] Reference [47], first-principles calculation. [i] Reference [50], Miedema's semi-empirical model.

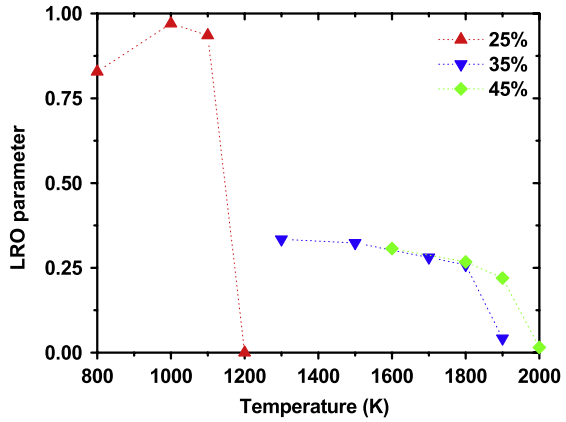

Figure 4. Temperature dependence of the long-range order (LRO) parameter for bcc Fe–Al alloys with 25, 35 and 45 at.% Al, obtained from a Monte Carlo simulation. The LRO value of 1 corresponds to a perfect DO3 ordering while a value of 0.33 corresponds to B2 ordering at individual compositions.

potential certainly reproduces the order/disorder transitions that occurs in the bcc Fe–Al alloys reasonably well. Now, the calculation was extended to the defect (vacancy or anti-site atom) formation energy in a perfect B2 ordered structure. Defect formation energy is defined as the energy difference between a system containing a defect and a perfect system with the same number of atoms:

$$E_f^{defect} = E^{defect}(N_{Fe} + N_{Al}) - (N_{Fe}\mu_{Fe} + N_{Al}\mu_{Al}). \quad (10)$$

E^{defect} is the potential energy per atom of the system containing a defect, N_{Fe} and N_{Al} the number of individual atoms, and μ_{Fe}, μ_{Al} the atomic chemical potentials of individual elements. The atomic chemical potential can be calculated by a numerical differentiation of the energy versus composition curve at 0 K. According to our calculation, the atomic chemical potential of Fe and Al is −4.722 and −3.524, respectively. The calculated vacancy and anti-site formation energies in the Fe and Al sites are listed in table 7, in comparison with experimental data and other calculations. The experimental information is available only for vacancy formation energy in the Fe site. The scattering among various calculations is large. However, all show qualitative agreement in that vacancy formation in Al sites is energetically most unfavorable, and the present calculations are in the scattering range.

Based on the calculations for the order–disorder transition and point defect energy in the B2 ordered structure, it is believed that various defect evolutions in high Al (non-stoichiometric B2 ordered) Fe–Al alloys can be predicted with a reasonable accuracy using the atomistic approach. However, the eventual purpose of the atomistic studies is to utilize the atomistic simulation technique for understanding the effect of Al and various defects on the deformation behavior of steels. For this, it is further necessary to know the formation behavior of other defects that have an effect on the deformation behavior and interactions between them. In the present study, the effect of Al content on the stacking fault energy of fcc Fe, which is regarded to be closely related to twin formation, the grain boundary segregation of Al atoms in bcc Fe and the interaction between an Al atom and dislocations, are selected.

The stacking fault energy is calculated by comparing the total energy a faulted sample involving a stacking fault to that of a perfect sample with the same number of atoms. A perfect sample of the fcc Fe was prepared by depositing {111} atomic layers of a size of about 6.4 × 6.6 nm^2 to a height of about 22 nm. The number of atoms was about 79 000. Al atoms up to 20 at.% were randomly distributed. A single layer intrinsic stacking fault was created by removing one atomic layer from the perfect fcc stacking of {111} planes. The total energy of the perfect and faulted samples was calculated by a molecular statics (MS) simulation applying a three-dimensional periodic boundary condition and allowing full relaxations of individual atoms, and also the sample dimension in all directions. Figure 5 shows the calculated effect of addition of Al to the intrinsic SFE in fcc Fe. The SFE in pure fcc Fe is set to be zero. According to the present calculation, the SFE of fcc Fe monotonically increases with increasing Al content, in qualitative agreement with experimental perception.

To investigate the tendency of Al atoms on grain boundaries to segregate, the above-mentioned MC simulation that has been used to investigate the order/disorder transition was performed again over alloy samples (of about 6 × 6 × (10–13) nm^3 with 35 000–37 000 atoms) involving an arbitrarily selected tilt or twist boundary. After the MC runs, the concentration profile of Al across the boundary was calculated. The results obtained for bcc Fe–20 at.% Al alloys at 873 K are plotted in figures 6(a) and (b), in comparison with initial concentration profiles. When compared to initial concentration profiles, the segregation on the grain boundaries looks small, especially on the tilt grain boundary that has a relatively compact atomic structure. The present authors are not aware of any quantitative experimental information for

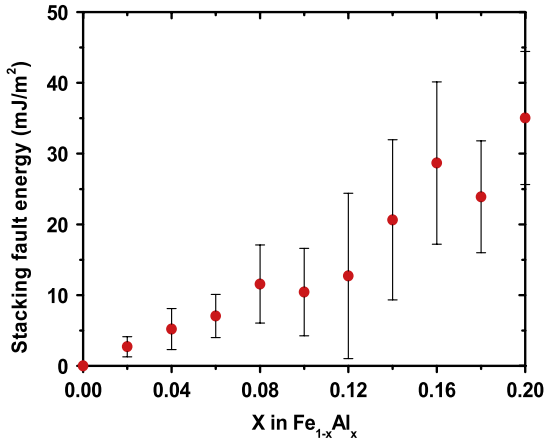

Figure 5. Calculated effect of Al content on the intrinsic stacking fault energy of fcc Fe. The stacking fault energy of pure Fe is set to zero.

Table 8. Calculated binding energy between an edge or screw dislocation and an Al atom in bcc Fe. The unit of the energy is eV.

	Edge	Screw
MEAM	0.16	0.14

the grain boundary segregation of Al atoms in steels. The present atomistic simulation study predicts a small segregation tendency of Al atoms on the grain boundaries in bcc Fe. Further simulation for a wider range of grain boundaries and temperatures would be necessary to provide more quantitative information.

Finally, the binding energy between an edge or a screw dislocation and an Al atom in bcc Fe was investigated using the present atomistic approach to estimate the effect of Al atoms on the movement of dislocations. The binding energy between a dislocation and a solute atom is defined as the energy difference between when a solute atom is located in the energetically most favorable site close to the dislocation and when it is far away from the dislocation. A positive value of the binding energy means that the two defects, a dislocation and a solute atom, are attractive. The calculated binding energies with the two different types of dislocation (edge and screw) are positive and of a similar size, as shown in table 8, which indicates a possibility of solution hardening due to the Al solute atoms in steels even though no quantitative experimental information is known.

For the moment, direct comparisons of the present calculations for the SFE, grain boundary segregation and interaction between dislocations and Al atoms with relevant experimental information and evaluation of the reliability of the present calculations may be difficult. This is because corresponding experimental information is not known quantitatively, and even when some qualitative information is available it is for multicomponent steels instead of the Fe–Al binary alloys. However, all the calculated properties are in a qualitative agreement with well accepted perceptions, and at least mutual comparisons for the effect on the SFE, grain boundary segregation tendency and interaction with dislocations between different alloying elements in steels can

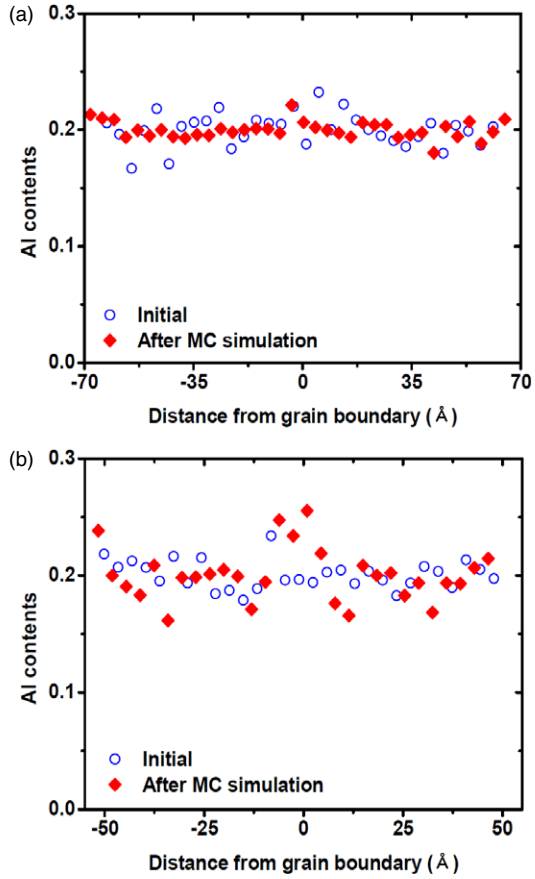

Figure 6. Concentration profile of Al across (a) tilt and (b) twist boundaries in bcc Fe–20 at.% Al alloys, obtained from a Monte Carlo simulation.

be easily made. The strongest advantage of the present MEAM approach is that all the above-mentioned properties can be investigated for practical Fe–Mn–Al–C multicomponent alloys since the Fe–C and Fe–Mn potentials are already available and can be easily combined into the quaternary potential.

4. Conclusion

It has been shown that the present 2NN MEAM interatomic potential for the Fe–Al system can reproduce structural, elastic and thermodynamic properties of Fe–Al binary alloys in generally good agreement with experimental information. The DO_3 or B2 ordering, point defect formation, stacking fault energy, grain boundary segregation and interactions between dislocations and solute atom are also reasonably reproduced. The present potential can be easily extended to more practical Fe–Al–Mn–C alloy system, and be applied to atomic level investigations of various defect formation behaviors and their effects on the mechanical properties of practical steels as well as Fe–Al binary alloys.

Acknowledgment

This work has been financially supported by the Pohang Steel Company (POSCO), Korea.

References

[1] Frommeyer G and Brüx U 2006 *Steel Res. Int.* **77** 627
[2] Kim Y G, Park Y S and Han J K 1985 *Metall. Trans.* A **16A** 1689
[3] Frommeyer G, Brux U and Neumann P 2003 *Iron Steel Inst. Japan Int.* **43** 438
[4] Westbrook J H and Fleischer R L 1994 *Intermetallic Compounds: Principles and Practice* (New York: Wiley)
[5] Fleischer R L, Dimiduk D M and Lipsitt H A 1989 *Annu. Rev. Mater. Sci.* **19** 231
[6] Reimann U and Sauthoff G 1999 *Intermetallics* **7** 437
[7] Machlin E S 1974 *Acta Metall.* **22** 95
[8] Matysina Z A, Pogorelova O S, Zaginaichenko S Y and Schur D V 1995 *J. Phys. Chem. Solids* **56** 9
[9] Crawford R C 1977 *Phil. Mag.* **35** 567
[10] Bichara C and Inden G 1991 *Scr. Metall. Mater.* **25** 2607
[11] Vailhe C and Farkas D 1997 *Acta Mater.* **45** 4463
[12] Besson R and Morillo J 1997 *Phys. Rev.* B **55** 193
[13] Shu X, Wangyu H U, Xiao H, Deng H and Zhang B 2001 *J. Mater. Sci. Technol.* **17** 601
[14] Lee B-J and Baskes M I 2000 *Phys. Rev.* B **62** 8564
[15] Lee B-J, Baskes M I, Kim H and Cho Y K 2001 *Phys. Rev.* B **64** 184102
[16] Lee B-J, Shim J-H and Baskes M I 2003 *Phys. Rev.* B **68** 144112
[17] Kim Y-M, Shin Y-H and Lee B-J 2009 *Acta Mater.* **57** 474
[18] Lee B-J and Lee J W 2005 *Calphad* **29** 7
[19] Lee B-J 2006 *Acta Mater.* **54** 701
[20] Rose J H, Smith J R, Guinea F and Ferrante J 1984 *Phys. Rev.* B **29** 2963
[21] Baskes M I 1992 *Phys. Rev.* B **46** 2727
[22] Baskes M I 1997 *Mater. Chem. Phys.* **50** 152
[23] Pearson W B 1958 *A Handbook of Lattice Spacing and Structures of Metals and Alloys* (Oxford: Pergamon)
[24] Taylor A and Jones R M 1958 *J. Phys. Chem. Solids* **6** 16
[25] Lihl F and Ebel H 1961 *Arch. Eisenhuettenwes.* **32** 483
[26] Leamy H J, Gibson E D and Kayser F X 1967 *Acta Metall.* **15** 1827
[27] Simmons G and Wang H 1971 *Single Crystal Elastic Constants and Calculated Aggregated Properties* (Cambridge: MIT Press)
[28] Breuer J, Grün A, Sommer F and Mittemeijer E J 2001 *Metall. Mater. Trans.* B **32B** 913
[29] Olsen W and Middel W 1937 *Eisenforschung* **19** 1
[30] Kubaschewski O and Dench W A 1955 *Acta Metall.* **3** 339
[31] Wooley F and Elliott J F 1967 *Trans. AIME* **239** 1872
[32] Petrushevsky M S, Esin Y, Gel'd P V and Sandakov V M 1972 *Russ. Metall.* **6** 149
[33] Sundman B, Ohnuma I, Dupin N, Kattner U R and Fries S G 2009 *Acta Mater.* **57** 2896
[34] Würchum R, Grupp C and Schaefer H-E 1995 *Phys. Rev. Lett.* **75** 97
[35] Rivière J P and Grilhé J 1975 *Scr. Metall.* **9** 967
[36] Lechermann F, Fähnle M and Sanchez J M 2005 *Intermetallics* **13** 1096
[37] Connétable D and Maugis P 2008 *Intermetallics* **16** 345
[38] Liu S, Duan S and Ma B 1998 *Phys. Rev.* B **58** 9705
[39] Gonzales-Ormeño P G, Petrilli H M and Schön C G 2002 *Calphad* **26** 573
[40] Sodré N, Gonzales-Ormeño P G, Petrilli H M and Schön C G 2009 *Calphad* **33** 576
[41] Fu C L and Yoo M H 1992 *Acta Metall. Mater.* **40** 703
[42] Das G P, Rao B K and Jena P 2002 *Phys. Rev.* B **66** 184203
[43] Kim H 2009 private communication
[44] Kellou A, Grosdidier T, Raulot J M and Aourag H 2008 *Phys. Status Solidi* b **245** 750
[45] Kellou A, Feraoun H I, Grosdidier T, Coddet C and Aourag H 2004 *Acta Mater.* **52** 3263
[46] Fu C L, Ye Y-Y, Yoo M H and Ho K M 1993 *Phys. Rev.* B **48** 6712
[47] Fähnle M, Mayer J and Meyer B 1999 *Intermetallics* **7** 315
[48] Kim J, Koo Y and Lee B-J 2006 *J. Mater. Res.* **21** 199
[49] Kim Y-M and Lee B-J 2008 *J. Mater. Res.* **23** 1095
[50] Bakker H, Modder I W and Kuin M J 1997 *Intermetallics* **5** 535